DR. HONG-WEI XUE (Orcid ID : 0000-0002-7641-5320)

Article type : Research Article

Rice microtubule-associated protein IQ67-DOMAIN14 regulates rice grain shape by modulating microtubule cytoskeleton dynamics

BaoJun Yang[1,3,4], Jos R. Wendrich[2,3,4], Bert De Rybel[3,4,*], Dolf Weijers[2,*] and Hong-Wei Xue[1,5,*]

[1]National Key Laboratory of Plant Molecular Genetics, CAS Center for Excellence in Molecular Plant Sciences, Shanghai Institute of Plant Physiology and Ecology, Chinese Academy of Sciences, 300 Fenglin Road, 200032 Shanghai, China

[2]Laboratory of Biochemistry, Wageningen University, Stippeneng 4, 6708 WE Wageningen, The Netherlands

[3]Ghent University, Department of Plant Biotechnology and Bioinformatics, Technologiepark 71, 9052 Ghent, Belgium

[4]VIB Center for Plant Systems Biology, Technologiepark 71, 9052 Ghent, Belgium

[5]School of Agriculture and Biology, Shanghai Jiao Tong University, 800 Dongchuan Road, 200240 Shanghai, China

[*]**Authors for correspondence:**

Email:

Hong-Wei Xue: hwxue@sibs.ac.cn,

Dolf Weijers: dolf.weijers@wur.nl,

Bert De Rybel: beryb@psb.vib-ugent.be

This article has been accepted for publication and undergone full peer review but has not been through the copyediting, typesetting, pagination and proofreading process, which may lead to differences between this version and the Version of Record. Please cite this article as doi: 10.1111/PBI.13279

Running head: OsIQD14 regulates MT rearrangement and grain shape

Key words: calmodulin (CaM), cell shape, microtubule, OsIQD14, rice

Summary

Cortical microtubule (MT) arrays play a critical role in plant cell shape determination by defining the direction of cell expansion. As plants continuously adapt to ever-changing environmental conditions, multiple environmental and developmental inputs need to be translated into changes of the MT cytoskeleton. Here, we identify and functionally characterize an auxin-inducible and MT-localized protein OsIQ67-DOMAIN14 (OsIQD14), which is highly expressed in rice seed hull cells. We show that while deficiency of *OsIQD14* results in short and wide seeds and increases overall yield, overexpression leads to narrow and long seeds, caused by changed MT alignment. We further show that OsIQD14-mediated MT reordering is regulated by specifically affecting MT dynamics, and ectopic expression of OsIQD14 in *Arabidopsis* could change the cell shape both in pavement cells and hypocotyl cells. Additionally, OsIQD14 activity is tightly controlled by calmodulin proteins, providing an alternative way to modify the OsIQD14 activity. Our results indicate that OsIQD14 acts as a key factor in regulating MT rearrangements in rice hull cells and hence the grain shape, and allows effective local cell shape manipulation to improve the rice yield trait.

Introduction

Rice (*Oryza sativa*) is one of the most important food crops for nearly half of the world population. Control of plant shape and architecture has been a major topic in rice plants and has great potential for crop yield improvement (Gupta *et al.*, 2006). Specifically grain size, controlled by the length and width of the grain, is a key factor determining final yield and is mainly restricted by spikelet hull size (Zuo & Li, 2014). Many genes controlling grain size have been identified in rice and recent studies have shown that this trait is controlled by multiple signaling pathways involving phytohormones, G-proteins, and ubiquitin-mediated proteasomal degradation pathways (Zuo & Li, 2014; Li & Li, 2016). Despite these advances, it remains largely unknown how these pathways control the spikelet hull size at cellular level.

Microtubule (MTs) dynamics and the cytoskeleton in general play an important role in plant morphogenesis (Hashimoto, 2015). Ordered cortical MT arrays play a critical role in plant cell shape formation by defining the axis of cell expansion through control of cellulose orientation and cell wall organization. As a result, MT organization determines directional cell expansion and plant morphogenesis (Baskin, 2001; Paredez *et al.*, 2006; Gutierrez *et al.*, 2009). However, due to pleiotropic effects upon MT modification, it is challenging to exploit MT array organization for crop improvement. Many MT associated proteins (MAPs) play vital roles in organizing the MT cytoskeleton and cell shape formation (Hashimoto, 2015). Nevertheless, how these proteins cooperatively regulate MTs dynamics and how they integrate multiple environmental and developmental signals to control cell morphogenesis and plant shape, remains a major unanswered question in plant biology.

Recently, the plant-specific IQ67-DOMAIN (IQD) family emerged as regulators of fruit shape and grain size in several plant species including tomato (Xiao *et al*., 2008), watermelon (Duo *et al*., 2018), cucumber (Pan *et al.*, 2017) and rice (Duan *et al.*, 2017; Liu *et al.*, 2017). For example, the tomato *SUN* gene encodes a member of IQD family and is involved in regulating fruit shape. Increased *SUN* expression led to elongated tomato shape (Xiao *et al*., 2008). Similar elongated fruit shape was found in watermelon and cucumber, associated with high IQD expression, suggesting that a conserved mechanism may exist for IQD-mediated fruit shape regulation. However, their precise biological roles and biochemical functions remain to be elucidated, especially in crop plants. IQD proteins contain a conserved, 67 amino acid domain and were first identified in *Arabidopsis* where it is represented by a 33-member gene family (Abel *et al.*, 2005).

Evidence form *Arabidopsis* showed that IQDs play important roles in leaf shape determination and xylem secondary cell wall architecture (Burstenbinder *et al.*, 2017; Sugiyama *et al*., 2017; Liang *et al*., 2018). Most of the *IQD* genes have distinct expression patterns, preferentially in embryo, stomata, meristematic cells and elongating tissues (Wendrich *et al*., 2018; Burstenbinder *et al*., 2017). Previous studies also showed that IQD proteins can associate with microtubules or the plasma membrane, and can interact with Calmodulin proteins through their IQ67 domain (Levy *et al*., 2005; Burstenbinder *et al.*, 2013; Burstenbinder *et al*., 2017). However, the biological relevance of interaction with Calmodulins remains unknown. Furthermore, while a function for plasma membrane-localized IQD proteins have been suggested in rice (Duan *et al*., 2017; Liu *et al*., 2017), the role of MT-localized IQD proteins remains elusive.

In this study, we identified OsIQD14 as a MT-localized IQ-domain containing protein, which is highly expressed in rice seed hull cells. Loss-of-function of OsIQD14 results in short and wide seeds with increased weight, while OsIQD14 overexpression leads to narrow and long seed without effect on seed weight. We further show that OsIQD14 activity is inhibited by Calmodulins and provide mechanistic evidence that OsIQD14 alters cell shape by affecting MT ordering. In conclusion, these results show that dynamic regulation of MTs by OsIQD14 can be used to manipulate the cell shape and yield in rice.

Results

OsIQD14 is Auxin-inducible and Transcribed during Seed Hull Development

Considering that the *Arabidopsis* AtIQD15-18 subclade, acting downstream of the AUXIN RESPONSE FACTOR5/MONOPTEROS (ARF5/MP) transcription factor (Möller *et al.*, 2017), is represented by a single OsIQD14 ortholog in rice (Abel *et al.*, 2005), we analyzed its expression pattern using the transcript digital gene chip. We found *OsIQD14* to be highly expressed in inflorescences, pistils, and spikelet hull tissues (Figure S1a), indicating that *OsIQD14* may have potential roles in grain size regulation. Quantitative RT-PCR (qRT-PCR) analysis further showed that *OsIQD14* transcripts can be detected during panicle development, peaking around the middle stage and gradually decreasing in mature stages of development, confirming *OsIQD14* is expressed highly in the inflorescence (Figure 1a). We further analyzed the expression pattern by fusing the *OsIQD14* promoter region to the ß-glucuronidase (GUS) reporter. Young spikelet hulls and anthers showed a strong GUS signal (Figure 1b-1d), indicating that *OsIQD14* may play a role during rice spikelet hull development. As some of the *Arabidopsis* orthologs were reported to be auxin-inducible (Möller *et al.*, 2017), we analyzed *OsIQD14* transcript levels upon exogenous auxin treatment. qRT-PCR analysis confirmed that *OsIQD14* transcripts were quickly induced upon auxin (Indole 3-Acetic Acid, IAA) treatment (Figure 1e), suggesting that *OsIQD14* may also be transcriptionally regulated by ARFs in rice.

OsIQD14 Controls Grain Dimensions by Regulating Spikelet Hull Cell Shape

To define the biological function of *OsIQD14*, we generated loss-of-function mutants by using CRISPR/Cas9 technology (Miao *et al.*, 2013). A construct expressing a guide RNA targeting the first exon of *OsIQD14* was transformed into ZH11 wild type (WT) rice plants. Five independent homozygous lines were isolated that carried frame shift mutations resulting from a 1-bp (*iqd14-1*) insertion or a 5-bp (*iqd14-2*), 22-bp (*iqd14-3*), 34-bp (*iqd14-4*) or 3-bp (*iqd14-5*) deletion, respectively (Figure S1b). None of the independent mutants presented a visible phenotype during vegetative growth, but four of them (except the 3-bp deletion line *iqd14-5*) produced wider and shorter grains compared to those of ZH11 (Figures 2a-b, d-e and Figure S1c, d), demonstrating a role for *OsIQD14* in panicle and spikelet development. The 3-bp deletion line (*iqd14-5*) result in a single amino acid deletion without visible phenotypes, suggesting that the phenotype observed in

other four frame shift mutations is not due to off-target effects. For all further analyses, the 5-bp deletion *iqd14-2* mutant allele (labeled as *iqd14-C*) was selected.

To determine if OsIQD14 was not only necessary, but also sufficient for regulating grain shape, we next generated overexpression plants by driving *OsIQD14* from the strong p35S promoter in a ZH11 background (p35S::OsIQD14:GFP). In contrast to the ZH11 and *iqd14-C* mutant, plants overexpressing *OsIQD14* produced narrower and longer grains (Figures 2c, f and g-h). Furthermore, the 1000-grain weight of *iqd14-C* was significantly increased compared to that of ZH11, while that of p35S::OsIQD14:GFP was similar to ZH11 (Figure 2i). Importantly, the panicle of *iqd14-C* and p35S::OsIQD14:GFP was similar to that of ZH11 (Figure 2j).

As the spikelet hull has been proposed to restrict growth of a grain and as such to determine grain size, we examined epidermal morphology of individual spikelet hull cells in the outer and inner glume of the lemma of ZH11, *iqd14-C* and p35S::OsIQD14:GFPplants. Scanning electron microscopy (SEM) analysis revealed that *iqd14-C* spikelet hull cells were shorter and wider than that of ZH11 (Figures 3a-b, d-e and Figures 3j-k). Conversely, the hull cells of p35S::OsIQD14:GFP plants were narrower and longer than those of ZH11 and *iqd14-C* plants (Figures 3c, f, i). Although *iqd14-C* showed a decreased hull cell length and p35S::OsIQD14:GFP plants presented promoted hull cell elongation (Figure 3m), they both showed decreased hull cell numbers (Figure 3n), suggesting the altered seed shape is due to the hull cell shape alterations, but not due to OsIQD14-mediated cell division control. Further counting the cell numbers in the spikelet hull of *iqd14-C* and p35S::OsIQD14:GFP plants in the grain-width direction confirmed that there was no difference compared to that of ZH11 (Figure 3o). Taken together, these results indicate that the changes in overall seed shape by modifying *OsIQD14* levels (e.g. short and wide versus long and slender) are caused by the same type of changes to the individual spikelet hull cells, and that modifying *OsIQD14* transcript levels can be used as a tool to modify rice grain shape without a yield penalty under normal growth conditions.

OsIQD14 is a Microtubule-binding Protein

To understand through what mechanism OsIQD14 can alter the cell shape, we first analyzed its subcellular protein localization. Similar to some IQD proteins in *Arabidopsis* (Burstenbinder *et al.*, 2013; Burstenbinder *et al.*, 2017), OsIQD14:GFP fusion protein is localized to cytoskeleton-related structures in rice root cells (Figure 4a and S2d) and leaves cells (Figure 4b, c). Similar results were observed by transiently expressing OsIQD14:GFP fusion protein in *Nicotiana*

benthamiana epidermal cells (Figure S2a). Considering that the cytoskeleton-associated localization was abolished by application of the MT depolymerization drug oryzalin (Figure 4d-f), OsIQD14 thus likely localizes to MT. To better understand this MT-associated localization, we used super resolution Structured Illumination Microscopy (SIM) in *Arabidopsis* root meristem cells. Intriguingly, we observed the punctate localization of OsIQD14 along MTs (Figure S2b), while general MT associated proteins (p35S::MAP4:GFP, Mei *et al.*, 2012) showed uninterrupted distribution along the filaments (Figure S2c). This result suggests that OsIQD14 is not a generic MT binding protein, but associates with MT at specific positions.

To examine whether OsIQD14 interacts with MT directly, we performed a MT spin-down assay. Similar to MAP2, a generic MT-binding protein and positive control (Lewis *et al.*, 1988), OsIQD14 was detected in the pellet fraction (Figure 4g), demonstrating that OsIQD14 directly binds MT.

To elucidate which part of the OsIQD14 protein localized to MT, we generated GFP fusion proteins consisting of only the N- or C-terminal region of OsIQD14. Although both MT and nuclear localization were observed in the p35S::OsIQD14:GFP line expressing the full-length protein in dividing cells (Figures S2d), the C-terminal region of OsIQD14 fused to GFP showed MT localization only, while the N-terminal region of OsIQD14 fused to GFP showed nuclear localization only (Figure S3a-3h), suggesting that in dividing cells, OsIQD14 could bind to some unknown protein by its N terminus to mediate the nuclear localization. Taken together, these results show that OsIQD14 binds MT directly through its C-terminal domain.

In addition, We transformed both p35S::OsIQD14-C:GFP and p35S::OsIQD14-N:GFP into *Arabidopsis* and rice, but none of them showed difference compared to wild type plants (pavement cell shape in *Arabidopsis* or seed size in rice). These results suggested that full length IQD14 protein is necessary to affect grain size.

OsIQD14 Controls Cell Shape by Modulating Microtubule Behavior

We wondered whether and how OsIQD14 could change the MTs behavior and dynamics. Based on the results described above and cortical MTs localization of OsIQD14 in rice root cells and young leaves cells, it is also tempting to speculate that OsIQD14 controls spikelet hull cell shape by modifying the MT cytoskeleton. Unfortunately, the hardened spikelet hull cells in rice made observing MT ordering and dynamics technically impossible in our hands. Given that localization of the OsIQD14:GFP protein is conserved when expressed in *Arabidopsis* root and hypocotyl cells

(Figure S2b), we used *Arabidopsis* as a heterologous system to analyze the dynamics and function of OsIQD14. Similar to *AtIQD16* (Burstenbinder *et al.*, 2017), *Arabidopsis* seedlings expressing p35S::OsIQD14:GFP showed narrow, long and spiraling cotyledons (Figures 5a-b). Also, epidermal pavement cells became largely isodiametric and lost the typical jigsaw puzzle shape found in control plants (Figures 5c, d). A similar effect on cell shape was observed for the spikelet hull cells themselves in rice (Figure 3j-i). These results indicate that we can indeed use *Arabidopsis* as a good model system to analyze OsIQD14 dynamics and function. Intriguingly, MT topology was strongly affected in p35S::OsIQD14:GFP plants compared to control plants as visualized by using p35S::GFP:TUA6 marker lines (Figures S4a-b), indicating that OsIQD14 also affects MT orientation. Moreover, hypocotyls of the dark-grown p35S::OsIQD14:GFP seedlings were highly sensitive to Oryzalin (Figure 5e-f), further supporting the role of OsIQD14 in controlling MT stability (Nakamura et al., 2004; Komaki et al., 2010). Further analysis of whether *OsIQD14* overexpression could change the cell shape of *Arabidopsis* hypocotyl cells showed the much elongated hypocotyl cells of *Arabidopsis* lines expressing OsIQD14 (p35S::OsIQD14:GFP) compared to those of TUA6 marker line (p35S::GFP:TUA6, Figure S4c-S4e), similar to AtIQD16 (Burstenbinder et al., 2017), an confirming the OsIQD14 effects on cell shape.

To further investigate how OsIQD14 could change the MT array, we introduced an RFP-labeled MT marker (p35S::RFP:TUA6) into the p35S::OsIQD14:GFP line. We next analyzed MT dynamics in the presence or absence of OsIQD14 protein in dark-grown hypocotyl cells using spinning disk confocal microscopy and observed that OsIQD14 overexpression strongly reduced MT dynamics (Figures S5b and Movies S1-2). To further investigate how OsIQD14 could reduce the MT dynamics, we analyzed time lapse movies in more detail (Figures S5c-h). OsIQD14 overexpression caused more catastrophe events, with long time extension and more shrinking events (Figure S5d and Movies S3-4), which we quantified by kymograph analysis (Figures S5e-i). Furthermore, co-localization of OsIQD14 with MTs showed punctate localization of OsIQD14 along MTs (Figure S5d and Movies S3-4), implying that OsIQD14 could interact with a microtubule-associated protein to change MT dynamics and orientation. Taken together, these results suggest that OsIQD14 reduces MT dynamics, which results in altered cell shapes.

Ca^{2+}-dependent Binding of Calmodulin to OsIQD14

As plants continuously adapt cell growth and expansion to ever-changing environmental conditions, multiple environmental (e.g. light) and developmental (e.g. hormones) inputs need to

be translated into changes of the MT cytoskeleton. Considering the important function of OsIQD14 in controlling MT dynamics, we questioned how OsIQD14 activity itself could be controlled. Previously, interactions between IQD proteins and Calmodulins have been reported (Levy *et al.*, 2005; Burstenbinder *et al.*, 2013; Burstenbinder *et al.*, 2017), but the biological significance of this binding remains unclear. Hence, we first tested the interaction between OsIQD14 and three rice Calmodulins, named OsCaM1, 2 and 3, all of which showed similar expression patterns to *OsIQD14* in digital gene expression analysis (Figure S6a-c). Y2H and BiFC analyses showed that OsCaM1, 2 and 3 interact with OsIQD14 both *in vitro* (Figure 6a) and *in vivo* at MT structures in tobacco leaf epidermal cells (Figure 6b-g). Similar to other IQDs in *Arabidopsis*, OsIQD14 interaction with OsCaM1 was enhanced by calcium treatment (Figure 6h). We next aimed to investigate the biological significance of the OsCaM1-OsIQD14 interaction. Introducing a p35S::OsCaM1 construct into the *Arabidopsis* p35S::OsIQD14:GFP plants reverted all phenotypes related to *OsIQD14* overexpression back to controls (Figures S7a-f). These included the long, narrow and spiraling cotyledons, and the absence of jigsaw-shaped epidermal pavement cells (Figures S7g-i). Taken together, these results suggest that the Ca^{2+}-dependent Calmodulin-Os*IQD14* interaction inhibits OsIQD14 activity. Interestingly, the CaM-binding and MT-localization properties are separable: the CaM-interacting IQ67 domain is located in the N-terminus of OsIQD14, while the C-terminus is sufficient for MT localization (Figure S3g). Thus, the OsIQD14 protein likely recruits CaM to MT filaments through these two binding modules. Considering that multiple environmental (e.g. light) and developmental (e.g. hormones auxin) induce transient increases in cytosolic Ca^{2+} (Harada *et al.*, 2003; Monshausen *et al.*, 2011), it is possible that this input will alter the activity of IQD protein by interacting with CaMs proteins, which in turn promotes MT dynamics to modify cell growth and expansion.

Discussion

Grain size and shape are key targets for rice improvement and invaluable agronomic traits. A range of grain size and/or shape regulators have been identified through studying natural variation or mutagenesis (Li and Li, 2016; Zheng et al., 2015). Identification of causal genes has revealed a clear role for transcription factors such as OsSPL16 (Wang *et al.*, 2015), OsSPL13 (Si *et al.*, 2016), OsGRF4 (Hu *et al.*, 2015), a TRM-containing protein GW7 (Wang *et al.*, 2015), an auxin-metabolism protein TGW6 (Ishimaru *et al.*, 2013), a plasma membrane localized IQD protein GW5 (Duan *et al.*, 2017; Liu *et al.*, 2017), among others.

While these functions are diverse, no coherent mechanistic framework has emerged for the cellular basis underlying the altered morphology. Importantly, although GW5 and GW5 like (GW5L, Tian *et al.*, 2018) share similarities with OsIQD14 regarding sequence and control of seed shape, both GW5 and GW5L are plasma membrane localized protein involving in brassinosteroid signaling by regulating BIN2 activity. In contrast, we identified OsIQD14 as a key regulator of grain shape by acting on cell shape determination through controlling the MT cytoskeleton, making this a novel target for breeding approaches. In addition, GW5 and GW5L were shown to regulate the grain width by limiting cell proliferation in the spikelet hull through regulating BIN2 activity, while our studies showed that MT-binding OsIQD14 changes the cell shape of rice hull, suggesting that cell shape modification could also change the grains size, which is different from GW5 or GW5L. Intriguingly, while mutations and overexpression of OsIQD14 consistently affect grain properties, no adverse pleiotropic effects were observed. Thus, OsIQD14 allows direct modulation of MT behavior and cell shape in husk cells to affect grain properties without the pleiotropic effects that manipulation of the MT cytoskeleton often induces (Hashimoto, 2015).

OsIQD14 is highly expressed in the rice panicle and SAM. However, when *OsIQD14* was overexpressed in *Arabidopsis*, we did not find obvious difference in the inflorescence, flowers or seeds. Considering the difference in plant architecture between monocots and dicots, this suggests that IQDs function differently in different plant species. Recent work on *Arabidopsis* IQDs showed that ectopic expression of *AtIQD16* also leads to narrow, long and spiraling cotyledons (Burstenbinder *et al*., 2017), suggesting that the basic function of IQDs in regulating MTs dynamics is likely conserved.

Auxin has been suggested to influence MT dynamics, but the mechanism is largely unknown (Chen *et al*., 2014). Recent studies showed that auxin-mediated embryonic root formation may

involve IQD proteins (Möller *et al*., 2017). OsIQD14 is the closest homolog of *Arabidopsis* AtIQD15-18 subclade, some of which are transcriptionally regulated by the AUXIN RESPONSE FACTOR5/MONOPTEROS (ARF5/MP) transcription factor (Möller *et al*., 2017). The expression of *OsIQD14* in rice was also induced by auxin, suggesting that rice and *Arabidopsis* IQDs may share a conserved upstream transcriptional regulatory mechanism. Experimental data from *Arabidopsis* provides evidence that auxin can mediate the microtubule reorganization within few minutes (Chen *et al*., 2014), and it will be interesting to test whether IQDs are involved in this rapid response. However, in our case, the hard hull cells of rice made it technically impossible to examine the microtubule dynamics. Using the *Arabidopsis* model to test the direct link between auxin/MTs and IQDs will expand our understanding of IQDs function on transferring signals to changes of the MT cytoskeleton. In addition, auxin can induce an increase of Ca^{2+} in few seconds (Monshausen *et al*., 2011), which could promote CaM binding to IQDs (Figure 6h). Intriguingly, we also found that OsIQD14 activity is regulated by CaMs (Figure S7). It is possible that high levels of Ca^{2+} will lead to the inhibition of IQD activity, which then regulates the behavior of microtubules. Given that similar activities and regulation were found for the *Arabidopsis* orthologs of OsIQD14 (Burstenbinder *et al.*, 2017), this module is likely deeply conserved in flowering plants.

Intriguingly, the phenotypes observed upon OsIQD14 overexpression in *Arabidopsis* seedlings are very similar to those observed in *spiral2* mutants (Shoji *et al*., 2005; Wightman *et al*., 2013). SPIRAL2 (SPR2) is a plant-specific MT binding protein required for anisotropic growth in *Arabidopsis* (Shoji *et al*., 2004, 2005; Wightman *et al*., 2013; Yao *et al*., 2008). Recent reports showed that SPR2 can protect MT minus ends to promote KATANIN-dependent severing and reorientation of plant cortical microtubule arrays (Nakamura *et al*., 2018). Our preliminary data from yeast two hybrid (Y2H) and bimolecular fluorescence complementation (BiFC) analyses suggested that there is a direct interaction between OsIQD14 and SPR2 (Wendrich *et al*., 2018). However, it remains unclear how these proteins regulate each other. Based on the identical spiraling phenotype observed in IQD14 overexpression lines and the *spr2* mutant, IQD14 might inhibit SPR2 activity. In *spr2* mutants, the MT reorientation induced by a blue light stimulus was abolished. Notably, blue light also can trigger a calcium flux within seconds (Babourina *et al*., 2002). It is thus likely that CaMs, IQDs and SPR2 might form a multimeric protein complex, allowing to regulate each other's activity. In this scenario, IQDs could inhibit SPR2 activity, which in turn could be blocked by calcium-mediated CaM binding to IQD14. Although it is

tempting to propose a central role for IQD proteins in this process, a more detailed analysis of this putative protein complex will be required to fully understand this auxin induced calcium flux and its link to microtubule reorientation in the coming years.

Experimental procedures

Plant Materials and Growth Conditions

Rice (*Oryza sativa*, *japonica* variety Zhonghua11, ZH11) plants were cultivated in the field at Shanghai under natural growing conditions. For growth of transgenic plants, rice seeds were germinated in sterilized water and grown in a phytotron under a 12-h light (28°C) / 12-h dark (22°C) cycle. *Arabidopsis thaliana* ecotype Columbia-0 (Col-0) was used in all transformation and phenotype analysis. All seeds were germinated on MS (Murashige and Skoog, Duchefa) medium after three days at 4^{o}C. Seedlings and plants were grown in a phytotron at 22^{o}C with a 16-h light/8-h dark photoperiod.

Vector Construction and Plant Transformation

The vector CRISPR/Cas9-*iqd14* was generated by using two 20-bp fragments from the first exon of OsIQD14 introducing into pOsCas9 vector, and then this plasmid was transformed into rice (ZH11) by *Agrobacterium tumefaciens*-mediated transformation (Hiei *et al.*, 1994). The OsIQD14 cDNA was amplified by PCR with primers IQD14-1 and IQD14-2 (Table S1) using total cDNA of ZH11 seedlings as template and subcloned into pENTR/D-TOPO (Invitrogen) to generate the pENTR/D-TOPO-IQD14 construct. For stable transformation, p35S::OsIQD14:GFP was generated by LR reactions with pGWB5 using pENTR/D-TOPO-IQD14, which was then transformed into ZH11. *OsIQD14* expression levels of p35S::OsIQD14:GFP plants were examined by qRT-PCR and confirmed positive lines were used for further analysis.

Transformation of *Arabidopsis* Col-0 plants was performed by the floral-dipping procedure. Plants expressing p35S::OsCaM1:RFP and p35S::OsIQD14:GFP were generated by introducing a p35S::OsCaM1:RFP construct into p35S::OsIQD14:GFP plants. Primers are listed in Supporting Information Table S1.

Promoter-reporter Gene Fusion Studies and GUS Activity Analysis

To analyze the expression pattern of *OsIQD14* gene, a 700-bp DNA fragment of *OsIQD14* promoter was amplified by PCR using ZH11 genomic DNA as template and subcloned into pENTR/D-TOPO vector. The resultant construct pOsIQD14::GUS was generated by LR reaction with pGWB4 and transformed into ZH11 and confirmed positive lines were used for further analysis. GUS activity of T2 homozygous progeny of independent lines were detected according to previous description (Jefferson *et al.*, 1987) and photographed using a Nikon SMZ 800 stereoscope with a Nikon digital Coolpix 995 camera.

RNA Extraction and Quantitative Real-time PCR (qRT-PCR) Analysis

Total RNAs were extracted using Trizol reagent (Invitrogen) and reversely transcribed to first-strand cDNA. qRT-PCR analysis was performed with Real-Time PCR Master Mix (Toyobo) and data were collected using the Bio-Rad Real Time detection system in accordance with the manufacturer's instruction manual. Primers were listed in Supporting Information Table S1. Expression of *OsIQD14* was analyzed using primers IQD14-RT1 and IQD14-RT2.

Scanning Electron Microscopy Observation of Spikelet Hull

Number and area of cells at the outer parenchyma layer of the spikelet hulls were measured by Olympus stream software. The sample pretreatment for scanning electron microscopy observation (S-3000N; Hitachi) was performed as described previously (Liu *et al.*, 2015). Grain weight was analyzed as described previously (Fu & Xue, 2010).

Subcellular Localization and Cell Shape Analysis

Fluorescence of transgene seedlings and tobacco epidermal cells was observed by confocal laser scanning microscopy (Leica SP8) with an argon laser excitation wavelength of 488 nm or 561 nm. For imaging with SIM, the Alpha Plan Apochromat 1003, NA 1.57 oil objective was used, and images were acquired from a single optical section.

For spikelet hull cell morphology analysis, PI (10 μg/ml) was applied to rice young spikelet cells, which were then imaged by confocal.

MT Dynamic Analysis

Confocal imaging for MT dynamic analysis was performed with a Perkin-Elmer spinning-disk confocal with a 100X Plan-Apo 1.4 NA oil-immersion objective. GFP was excited at 488 nm and

RFP was excited at 561 nm. The time series used for comparing MT dynamics were acquired by exciting RFP:TUA6 with 400 ms exposures of 561 nm excitation at 20 s intervals over 30 min. Time-lapse imaging for the OsIQD14:GFP and RFP:TUA6 dual-labeled plants was performed at 20 s time intervals with 500 ms exposures. To measure the MT dynamics, we color-coded the movies based on time (in which for example MT at frame 1 are red, MT at frame 6 green etc.). Hence, static MTs show as white structures (overlay of all colors: red, green, blue, cyan, magenta and yellow, corresponding to frames 1, 11, 21, 31, 41 and 51), while the mobile MT structures will be displayed as a multi-colored line.

Protein-protein Interaction Assays

Interaction of OsIQD14 and OsCaMs was detected by standard Y2H analysis following the manufacturer's instructions (Clontech). cDNAs encoding OsIQD14, OsCaM1, 2, 3 were subcloned into pGBKT7 and pGADT7 vector, resulting in the fusion of OsIQD14-AD, OsCaM1-AD, OsIQD14-BD, and OsCaM1-BD respectively (AD, activating domain; BD, binding domain). Primers are listed in Supporting Information Table S1. Yeast transformants were spotted on the restricted SD medium (SD-Leu/-Trp, short as SD-L/T) and selective medium (SD-Leu/-Trp/-His/, short as SD-L/T/H). For BiFC (Bimolecular Fluorescence Complementation) assay, cDNAs encoding *OsIQD14* or *OsCaM1* were cloned into p35S::YFP-N or p35S::YFP-C vector using modified BiFC vector (Ma *et al.*, 2016), resulting in constructs expressing OsIQD14-cYFP and OsCaM1-nYFP. Resultant constructs with control vectors were co-expressed in *N. benthamiana* leaves and YFP was observed by Leica SP8 confocal microscope using an argon laser excitation wavelength of 488 nm after infiltration for 3 days.

Recombinant Expression of OsIQD14 and MT Spin-Down Assay

Coding sequences of *OsIQD14* were amplified by PCR (primers *IQD14-COLD-P1/2*) and subcloned into pCold-HF for expression of OsIQD14-His fusion proteins. After confirmation by sequencing, the construct was transformed into *E. coli* BL21(DE3) cells, and expression of the fusion protein was induced by adding isopropyl-β-D-thiogalactoside (IPTG, final concentration 1 mM) at 16^{o}C overnight. The cells were lysed by sonication in lysis buffer (50 mM NaH_2PO_4, 300 mM NaCl and 10 mM imidazole, pH 8.0) and OsIQD14-His protein was purified using Ni-NTA His Bind Resin (Novagen) according to the manufacturer's protocols. *In vitro* MT binding assay was performed using MT binding protein spin-down assay kit (Cytoskeleton). Briefly, 5 μg

purified His-OsIQD14-His protein was incubated with 10 μg prepolymerized bovine brain tubulin in general tubulin buffer (80 mM PIPES, pH 7.0, 2 mM $MgCl_2$, and 0.5 mM EGTA) containing 20 μM taxol followed by centrifugation at 100,000g, and both soluble and pellet fractions were analyzed by SDS-PAGE and Coomassie Brilliant Blue staining.

Expression of Recombinant OsCaM1 and Calmodulin Binding Assay

Calmodulin binding assay were performed according to previous description with some modifications (Levy *et al.*, 2005). For expression of OsCaM1-GST, a full-length cDNA fragment encoding the OsCaM1 were first amplified and then subcloned into pENTR/D-TOPO (Invitrogen). To express the OsCaM1-GST fusion protein, pDEST-GST were used with Gateway LR Clonase II enzyme mix (Invitrogen). The recombinant OsCaM1 protein was expressed in BL21(DE3) at 30^{o}C for 4 h by induction with 1 mM IPTG. Bacterial cells were harvested and sonicated in Lysis buffer (50 mM Tris-HCL, 150 mM NaCl). After centrifugation, the supernatant was used for incubating with GST agarose. Aliquots of 100 μL of OsCaM1-GST beads, pre-equilibrated with Lysis buffer, were mixed with 500 μL of bacterial supernatant supplemented with 2 mM $CaCl_2$ or 5 mM EGTA and incubated for 1 hour at 4^{o}C under gentle shaking. OsCaM1 beads were sedimented by centrifugation and washed four times with 500 μL of Lysis buffer, followed by a final wash with 100 μL of the same solution. The bound proteins were eluted by boiling the beads for 2 min in 100μL of 4x SDS sample buffer. Proteins of the total extract, the initial supernatant, the last wash, and the pellet fraction were analyzed by SDS-PAGE and Western blot using antibody against His.

Author contributions

H.X. and D.W. conceived the project; B.Y. and J.R.W. designed experiments; B.Y. performed experiments; H.X., D.W. and B.D.R. supervised the project; B.Y., B.D.R., D.W. and H.X. wrote the paper with input from all authors.

Acknowledgements

Funding for this research is gratefully acknowledged from the National Key Research and Development Program of China (2016YFD0100902), the National Transformation Science and Technology Program (2016ZX08001006-009) and the National Natural Science Foundation of China (31671660). J.R.W. and D.W. were supported by the European Research Council (ERC; StG CELLPATTERN; 281573). B.Y. and B.D.R. were supported by the European Research Council (ERC; StG TORPEDO; 714055). We thank Ms. Shu-Ping Xu (SIPPE) for assisting with the rice transformation and acknowledge Daniël Van Damme for stimulating discussions.

Conflicts of interests

The authors declare no conflicts interests.

Supporting Information

Supporting information includes 7 figures, 1 table and 4 movies.

Figure S1. In silico expression profile of *OsIQD14* and analysis of *OsIQD14* CRISPR/Cas9 lines.

(a) *OsIQD14* digital expression levels in leaf, root, inflorescence, anther, pistil, lemma, palea, embryo and endosperm. (b) Targeted mutagenesis of *OsIQD14* gene. Position of target site is shown on the gene sequence. The spacer sequence is shaded in black. Sequencing results of mutant alleles are aligned to the reference genome sequence. (c) Seed phenotype of different mutagenesis of *OsIQD14* (Bar=1 cm). (d) Measurement and statistical analysis of length/width ratio of ZH11 and five different *iqd14* CRISPR/Cas9 lines. Data are shown as mean ± SE (n>300).

Figure S2. Subcellular localization of OsIQD14 protein.

(a) Subcellular localization of OsIQD14-GFP in *N. benthamiana* leaf epidermis cells (Z-stack projection; Bar=20 μm). (b-c) Super resolution structured illumination microscopy (SIM) analysis of p35S::OsIQD14:GFP and MAP4-GFP localization at microtubules in *Arabidopsis* root epidermis cells at meristem region. Bar=5 μm (b) or 10 μm (c). (d) Subcellular localization of OsIQD14-GFP in rice meristem dividing cells. Bar=10 μm.

Figure S3. Subcellular localizations of the N-terminus and C-terminus of OsIQD14.

(a-c) The N-terminal region of OsIQD14 (OsIQD14-N) fused to GFP is localized to the nucleus (Bar=20 μm) in *N. benthamiana* epidermis cells. (d-f) The C-terminal region of OsIQD14 (OsIQD14-C) fused to GFP is localized to microtubules (Bar=20 μm). (b, e) and (c, f) show the enlarged zone close to plasma membrane and nucleus (Bar = 10 μm or 5 μm respectively). (g-h) Root cells of 7-day-old transgenic *Arabidopsis* seedlings expression C terminal of OsIQD14-GFP (g, bar=5 μm) or N terminal of OsIQD14-GFP (h, bar=20 μm), which is localized to microtubules or nucleus, respectively.

Figure S4. OsIQD14 regulates cell shape of *Arabidopsis* by affecting microtubule ordering.

(a-b) Visualization of microtubule ordering in pavement cells using p35S::GFP:TUA6 in WT (Col-0) or p35S::OsIQD14:GFP (Bar=20 μm).

(c-d) Shape of hypocotyl cells of p35S::GFP:TUA6 and p35S::OsIQD14:GFP seedlings under light growth conditions. Bar=100 μm.

(e) Hypocotyl cell length of 7-day-old p35S::GFP:TUA6 and p35S::OsIQD14:GFP seedlings under light growth conditions. Data are shown as mean ± SE (n=50, P-value was calculated using a standard two-sided t-test; ***: $p<0.001$).

Figure S5. OsIQD14 affects MT behavior.

(a-b) Visualization of microtubule dynamic in dark grown hypocotyl cells using p35S::RFP:TUA6 in the absence (a) or presence (b) of p35S::OsIQD14:GFP with spinning disk confocal microscopy. Movies were color-coded based on time, the MT at frame 1 is red, the MT image at frame 6 is green etc. Dynamic MT is shown as multi-colored, while static MTs is shown as white (all colors overlaid on top of each other).

(c-d) A single MT labeled by p35S::RFP:TUA6 (c) and representative confocal time-lapse images of an MT extension and shrinking events showed that OsIQD14 (p35S::OsIQD14:GFP) alter the normal microtubule extension and shrinking time (d). Arrow heads in (c) and (d) indicate individual MT which is followed over time.

(e-h) Kymographs of p35S::RFP:TUA6 in etiolated hypocotyl cells in the absence (e) or presence (g, f) of p35S::OsIQD14:GFP. (Timeframe from 0s to 1800s; Bar=14 μm).

(i) Quantification of the plus end shrinking events in p35S::RFP:TUA6 in the absence or presence of p35S::OsIQD14:GFP (***, $p<0.001$, two-sided t-test, n=20).

Figure S6. In silico expression profile of *OsCaM1*, *2* and *3* in rice various tissues.

Digital expression levels of *OsCaM1* (a)*, OsCaM2* (b) and *OsCaM3* (c) in leaf, root, inflorescence, anther, pistil, lemma, palea, embryo and endosperm tissues of rice.

Figure S7. Pavement cell shape of *Arabidopsis* seedlings expressing *OsIQD14* and *OsCaM1*.

(a-f) Cotyledon phenotype of *Arabidopsis* Col-0, seedlings expressing OsCaM1 (p35S::CaM1), OsIQD14 (p35S::OsIQD14:GFP), and CaM1 and OsIQD14 seedlings (Bar=1 cm).

(g-j) Epidermal pavement cell phenotype of *Arabidopsis* Col-0, seedlings expressing OsIQD14 (p35S::OsIQD14:GFP), OsCaM1 (p35S::CaM1), and OaCaM1 and OsIQD14. PI was used to stain cell wall (Bar=50 μm).

Table S1. List of primers used in this study.

Movies are suggested to be viewed by "Storm video player"

Movie S1. Time series show the dynamic localization of RFP-TUA6 fusion protein (p35S::RFP:TUA6) in etiolated hypocotyl cells. Images were acquired at 20-s intervals.

Movie S2. Time series show the dynamic localization of RFP-TUA6 fusion protein (p35S::RFP:TUA6) in etiolated p35S::OsIQD14:GFP hypocotyl cells. Images were acquired at 20-s intervals.

Movie S3. Time series show the dynamic localization of OsIQD14-GFP fusion protein (green, p35S::OsIQD14:GFP) in etiolated hypocotyl cells. Images were acquired at 20-s intervals.

Movie S4. Time series show the dynamic localization of OsIQD14-GFP fusion protein (green, p35S::OsIQD14:GFP) and RFP-TUA6-labeled cortical MTs (red, p35S::RFP:TUA6) in dark-grown hypocotyl cells. Images were acquired at 20-s intervals.

References

Abel, S., Savchenko, T., Levy, M. (2005) Genome-wide comparative analysis of the IQD gene families in *Arabidopsis thaliana* and *Oryza sativa*. *BMC Evol. Biology* **5,** 72.

Babourina, O., Newman, I., Shabala, S. (2002) Blue light-induced kinetics of H^+ and $Ca2^+$ fluxes in etiolated wild-type and phototropin-mutant *Arabidopsis* seedlings. *Proc. Natl. Acad. Sci. USA* **99,** 2433-2438.

Baskin, T.I. (2001) On the alignment of cellulose microfibrils by cortical microtubules: a review and a model. *Protoplasma* **215,** 150-171.

Burstenbinder, K., Moller, B., Plotner, R., Stamm, G., Hause, G., Mitra, D., Abel, S. (2017) The IQD family of calmodulin-binding proteins links calcium signaling to microtubules, membrane subdomains, and the nucleus. *Plant Physiol.* **173,** 1692-1708.

Burstenbinder, K., Savchenko, T., Muller, J., Adamson, A.W., Stamm, G., Kwong, R., Zipp, B.J., Dinesh, D.C., Abel, S. (2013) *Arabidopsis* calmodulin-binding protein IQ67-domain 1 localizes to microtubules and interacts with kinesin light chain-related protein-1. *J. Bio. Chem.* **288,** 1871-1882.

Chen, X., Grandont, L., Li, H., Hauschild, R., Paque, S., Abuzeineh, A., Rakusova, H., Benkova, E., Perrot-Rechenmann, C., Friml, J. (2014) Inhibition of cell expansion by rapid ABP1-mediated auxin effect on microtubules. *Nature* **516**, 90-93.

Dou, J., Zhao, S., Lu, X., He, N., Zhang, L., Ali, A., Kuang, H., Liu, W. (2018) Genetic mapping reveals a candidate gene (ClFS1) for fruit shape in watermelon (*Citrullus lanatus* L.). *Theor. App. Genet.* **131,** 947-958.

Duan, P., Xu, J., Zeng, D., Zhang, B., Geng, M., Zhang, G., Huang, K., Huang, L., Xu, R., Ge, S., *et al.* (2017) Natural variation in the promoter of GSE5 contributes to grain size diversity in rice. *Mol. Plant* **10,** 685-694.

Fu, F.F., Xue, H.W. (2010) Coexpression analysis identifies Rice Starch Regulator1, a rice AP2/EREBP family transcription factor, as a novel rice starch biosynthesis regulator. *Plant Physiol.* **154,** 927-938.

Gupta, P.K., Rustgi, S., Kumar, N. (2006) Genetic and molecular basis of grain size and grain number and its relevance to grain productivity in higher plants. *Genome.* **49,** 565-571.

Gutierrez, R., Lindeboom, J.J., Paredez, A.R., Emons, A.M., Ehrhardt, D.W. (2009) *Arabidopsis* cortical microtubules position cellulose synthase delivery to the plasma membrane and interact with cellulose synthase trafficking compartments. *Nat. Cell Biol.* **11,** 797-806.

Hashimoto, T. (2015) Microtubules in plants. *Arabidopsis Book* **13,** 179.

Hiei, Y., Ohta, S., Komari, T., Kumashiro, T. (1994) Efficient transformation of rice (*Oryza sativa* L.) mediated by *Agrobacterium* and sequence analysis of the boundaries of the T-DNA. *Plant J.* **6,** 271-282.

Hu, J., Wang, Y., Fang, Y., Zeng, L., Xu, J., Yu, H., Shi, Z., Pan, J., Zhang, D., Kang, S., *et al.* (2015) A rare allele of GS2 enhances grain size and grain yield in rice. *Mol. Plant* **8,** 1455-1465.

Ishimaru, K., Hirotsu, N., Madoka, Y., Murakami, N., Hara, N., Onodera, H., Kashiwagi, T., Ujiie, K., Shimizu, B., Onishi, A., *et al.* (2013) Loss of function of the IAA-glucose hydrolase gene TGW6 enhances rice grain weight and increases yield. *Nat. Genet.* **45,** 707-713.

Jefferson, R.A., Kavanagh, T.A., Bevan, M.W. (198). GUS fusions - Beta-Glucuronidase as a sensitive and versatile gene fusion marker in higher plants. *EMBO J.* **6,** 3901-3907.

Komaki, S., Abe, T., Coutuer, S., Inze, D., Russinova, E., Hashimoto, T. (2010) Nuclear-localized subtype of end-binding 1 protein regulates spindle organization in *Arabidopsis*. *J. Cell Sci.* **123,** 451-459.

Levy, M., Wang, Q., Kaspi, R., Parrella, M.P., Abel, S. (2005) *Arabidopsis* IQD1, a novel calmodulin-binding nuclear protein, stimulates glucosinolate accumulation and plant defense. *Plant J.* **43,** 79-96.

Lewis, S.A., Wang, D.H., Cowan, N.J. (1988) Microtubule-associated protein MAP2 shares a microtubule binding motif with tau protein. *Science* **242,** 936-939.

Li, N., Li, Y. (2016) Signaling pathways of seed size control in plants. *Curr. Opin. Plant Biology* **33,** 23-32.

Liang, H., Zhang, Y., Martinez, P., Rasmussen, C.G., Xu, T., Yang, Z. (2018) The microtubule-associated protein IQ67 DOMAIN5 modulates microtubule dynamics and pavement cell shape. *Plant Physiol.* **177,** 1555-1568.

Liu, J., Chen, J., Zheng, X., Wu, F., Lin, Q., Heng, Y., Tian, P., Cheng, Z., Yu, X., Zhou, K., *et al.* (2017) GW5 acts in the brassinosteroid signalling pathway to regulate grain width and weight in rice. *Nat. Plants* **3,** 17043.

Liu, L.C., Tong, H.N., Xiao, Y.H., Che, R.H., Xu, F., Hu, B., Liang, C.Z., Chu, J.F., Li, J.Y., Chu, C.C. (2015) Activation of Big Grain1 significantly improves grain size by regulating auxin transport in rice. *Proc. Natl. Acad. Sci. USA* **112,** 11102-11107.

Ma, D.B., Li, X., Guo, Y.X., Chu, J.F., Fang, S., Yan, C.Y., Noel, J.P., Liu, H.T. 2016. Cryptochrome 1 interacts with PIF4 to regulate high temperature-mediated hypocotyl elongation in response to blue light. *Proc. Natl. Acad. Sci. USA*. **113,** 224-229.

Mei, Y., Gao, H.B., Yuan, M., Xue, H.W. (2012) The *Arabidopsis* ARCP protein, CSI1, which is required for microtubule stability, is necessary for root and anther development. *Plant Cell* **24,** 1066-1080.

Miao, J., Guo, D.S., Zhang, J.Z., Huang, Q.P., Qin, G.J., Zhang, X., Wan, J.M., Gu, H.Y., Qu, L.J. (2013) Targeted mutagenesis in rice using CRISPR-Cas system. *Cell Res.* **23,** 1233-1236.

Moller, B.K., Ten, Hove. C.A., Xiang, D.Q., Williams, N., Lopez, L.G., Yoshida, S., Smit, M., Datla, R., Weijers, D. (2017) Auxin response cell-autonomously controls ground tissue initiation in the early *Arabidopsis* embryo. *Proc. Natl. Acad. Sci. USA* **114,** 2533-2539.

Monshausen, G.B., Miller, N.D., Murphy, A.S., Gilroy, S. (2011) Dynamics of auxin-dependent Ca^{2+} and pH signaling in root growth revealed by integrating high-resolution imaging with automated computer vision-based analysis. *Plant J.* **65,** 309-318.

Nakamura, M., Naoi, K., Shoji, T., Hashimoto, T. (2004) Low concentrations of propyzamide and oryzalin alter microtubule dynamics in *Arabidopsis* epidermal cells. *Plant Cell Physiol.* **45,** 1330-1334.

Nakamura, M., Lindeboom, J.J., Saltini, M., Mulder, B.M., Ehrhardt, D.W. (2018) SPR2 protects minus ends to promote severing and reorientation of plant cortical microtubule arrays. *J. Cell Biol.* **217,** 915-927.

Pan, Y.P., Liang, X.J., Gao, M.L., Liu, H.Q., Meng, H.W., Weng, Y.Q., Cheng, Z.H. (2017) Round fruit shape in WI7239 cucumber is controlled by two interacting quantitative trait loci with one putatively encoding a tomato SUN homolog. *Theor. Appl. Genet.***130,** 573-586.

Paredez, A.R., Somerville, C.R., Ehrhardt, D.W. (2006) Visualization of cellulose synthase demonstrates functional association with microtubules. *Science **312,*** 1491-1495.

Shoji, T., Narita, N.N., Hayashi, K., Asada, J., Hamada, T., Sonobe, S., Nakajima, K., Hashimoto, T. (2004) Plant-specific microtubule-associated protein SPIRAL2 is required for anisotropic growth in *arabidopsis*. *Plant Physiol.* **136,** 3933-3944.

Shoji, T., Narita, N.N., Hayashi, K., Asada, J., Hamada, T., Sonobe, S., Nakajima, K., Hashimoto, T. (2005) Plant-specific microtubule-associated protein SPIRAL2 is required for anisotropic growth in *Arabidopsis*. *Plant Physiol.* **137,** 1169-1169.

Si, L.Z., Chen, J.Y., Huang, X.H., Gong, H., Luo, J.H., Hou, Q.Q., Zhou, T.Y., Lu, T.T., Zhu, J.J., Shangguan, Y.Y., *et al.* (2016) OsSPL13 controls grain size in cultivated rice. *Nat. Genet.* **48,** 447-453.

Sugiyama, Y., Wakazaki, M., Toyooka, K., Fukuda, H., Oda, Y. (2017) A novel plasma membrane-anchored protein regulates xylem cell-wall deposition through microtubule-dependent lateral inhibition of Rho GTPase domains. *Curr. Biol.* **27,** 2522-2528.

Tian, P., Liu, J., Mou, C., Shi, C., Zhang, H., Zhao, Z., Lin, Q., Wang, J., Wang, J., Zhang, X., *et al.* (2018) GW5-Like, a homolog of GW5, negatively regulates grain width, weight and salt resistance in rice, *J. Integr. Plant Biol.* doi: 10.1111/jipb.12745.

Wang, S., Li, S., Liu, Q., Wu, K., Zhang, J., Wang, S., Wang, Y., Chen, X., Zhang, Y., Gao, C., *et al.* (2015) The OsSPL16-GW7 regulatory module determines grain shape and simultaneously improves rice yield and grain quality. *Nat. Genet.* **47,** 949-954.

Wendrich, J.R., Yang, B.J., Mijnhout, P., Xue, H.W., De Rybel, B., Weijers, D. (2018) IQD proteins integrate auxin and calcium signaling to regulated microtubule dynamics during *Arabidopsis* development. *BioRxiv* **275560**.

Wightman, R., Chomicki, G., Kumar, M., Carr, P., Turner, S.R. (2013) SPIRAL2 determines plant microtubule organization by modulating microtubule severing. *Curr. Biol.* **23,** 1902-1907.

Xiao, H., Jiang, N., Schaffner, E., Stockinger, E.J., van der Knaap, E. (2008) A retrotransposon-mediated gene duplication underlies morphological variation of tomato fruit. *Science* **319,** 1527-1530.

Yao, M., Wakamatsu, Y., Itoh, T.J., Shoji, T., Hashimoto, T. (2008) Arabidopsis SPIRAL2 promotes uninterrupted microtubule growth by suppressing the pause state of microtubule dynamics. *J. Cell Sci.* **121,** 2372-2381.

Zheng, J., Zhang, Y.D., Wang, C.L. (2015) Molecular functions of genes related to grain shape in rice. *Breeding Science* **65:** 120-126.

Zuo, J.R., Li, J.Y. (2014) Molecular genetic dissection of quantitative trait loci regulating rice grain size. *Annu. Rev. Genet.* **48,** 99-118.

FIGURE LEGENDS

Figure 1. *OsIQD14* expression pattern.

(a) Quantitative RT-PCR (qRT-PCR) analysis revealed the transcription of *OsIQD14* in various tissues including SAM, leaf, and young panicles at different developmental stages (indicated as the lengths of panicles, cm). The expression levels were normalized with the *ACTIN* transcript and relative expression levels were calculated by setting the *OsIQD14* expression in leaf as "1.0". Experiments were biologically repeated and data are shown as mean ± standard error (SE).

(b-d) Promoter-GUS fusion analysis showed the *OsIQD14* expression in young panicle (0.4-cm in length) and lemma before anthesis of rice. Representative images are shown. Bar=2 mm.

(e) qRT-PCR analysis revealed the up-regulated expression of *OsIQD14* under short time (30 min - 420 min) auxin treatment (10 μM IAA). Rice seedling roots were used and expressions were normalized with the *ACTIN* transcript and relative expression levels were calculated by setting the *OsIQD14* expression in the absence of auxin as "1.0". Experiments were biologically repeated and data are shown as mean ±SE.

Figure 2. OsIQD14 regulates rice seed size.

(a-f) Grain morphology of ZH11 and rice transgenic plants deficiency of (*iqd14-C*) or overexpressing OsIQD14 (p35S::OsIQD14:GFP). Bar=20 mm.

(g-i) Measurement and statistical analysis of seed length and width (g), length/width ratio (h), and thousand-grain-weight (i) of ZH11, *iqd14-C* and p35S::OsIQD14:GFP plants. Data are shown as mean ± SE (n>300). Statistical analysis was performed by calculating the P-value using a standard two-sided t-test; ***, $p<0.001$; **, $p<0.01$; *: $p<0.05$.

(j) Harvested panicles of one plant individual in ZH11, *iqd14-C* and p35S::OsIQD14:GFP plants. Scale bar=2 cm.

Figure 3. *OsIQD14* regulates rice seed size by modifying hull cell shape.

(a-f) Scanning electron microscopy observation of seeds with hulls and outer glume (r-t bar=100 μm) of the lemma among ZH11, *iqd14-C* and p35S::OsIQD14:GFP plants. Bar=1 mm.

(g-i) Scanning electron microscopy observation of seeds without hulls of ZH11 (g), *iqd14-C* (h) and p35S::OsIQD14:GFP (i) plants (Bar=1 mm).

(j-l) Observation of cell shape inside hulls among ZH11 (j), *iqd14-C* (k) and p35S::OsIQD14:GFP (l) plants (Bar=50 μm).

(m-n) Measurement and statistical analysis of hull cell length (m) and hull cell number (n) of ZH11, *iqd14-C* and p35S::OsIQD14:GFP plants. Data are shown as mean ± SE (seeds, n=8; hull cells, n=125). Statistical analysis was performed by calculating the P-value using a standard two-sided t-test; ***, $p<0.001$; *, $p<0.05$.

(o) Measurement and statistical analysis of hull cell number in width direction of ZH11, *iqd14-C* and p35S::OsIQD14:GFP plants. Data are shown as mean ± SE (seeds, n=10). Statistical analysis was performed by calculating the P-value using a standard two-sided t-test.

Figure 4. OsIQD14 protein is located at microtubules.

(a-c) Subcellular localization of OsIQD14-GFP fusion protein in rice young root cells (a) or young leaves cells (b-c). Bar=10 μm.

(d-f) Subcellular localization of OsIQD14-GFP fusion protein in *Arabidopsis* hypocotyl cells under oryzalin treatment. Bar=7 μm.

(g) *In vitro* microtubule spin down assay showed that OsIQD14 binds to microtubules directly. OsIQD14-His protein was incubated without or with taxol-stabilized bovine MT (20 μM), divided into pellet (P) and soluble (Supernatant, S) fractions by ultracentrifugation, and then separated by 4-12% SDS-PAGE and stained with Coomassie brilliant blue. MAP2 protein (280 kDa) that binds to microtubules is used as positive control.

Figure 5. OsIQD14 regulates cell shape of *Arabidopsis* by affecting microtubule ordering.

(a-b) Seedling phenotype of wild type (Col-0) and *Arabidopsis* expressing p35S::OsIQD14:GFP (Bar=0.5 cm).

(c-d) Epidermal pavement cell phenotype of p35S::GFP:TUA6 in WT (Col-0) or *Arabidopsis* expressing p35S::OsIQD14:GFP (Bar=50 μm).

(e-f) Observation (e) and measurement (f) of hypocotyl lengths of dark grown 4-day-old wild type (Col-0) and *Arabidopsis* seedlings expressing p35S::OsIQD14:GFP under oryzalin treatment. Data are shown as mean ± SE (n=20). Statistical analysis was performed by calculating the P-value using a standard two-sided t-test; **, $p<0.01$.

Figure 6. Calmodulins interact with OsIQD14.

(a) Yeast-2-hybrid analysis showed that OsIQD14 interacts with OsCaM1, 2 and 3 directly *in vitro*. Full-length cDNAs of OsIQD14, OsCaM1, 2, 3 were subcloned into pGBKT7 or pGADT7 vectors. Transformed yeast cells were grown on synthetic dropout (SD-2, -Trp, -Leu; SD-3, -Trp, -His, -Leu) medium. Empty pGADT7 or pGBKT7 vectors transformed with OsIQD14-BD and OsCaM1/2/3-AD were used as negative controls. AD, activating domain; BD, binding domain.

(b-g) BiFC assay showed that OsIQD14 interacts with OsCaM1 at microtubules in *N. benthamiana* epidermis cells by co-expression of OsIQD14-n/cYFP and OsCaM1-c/nYFP (Bar =20 μm). (c) and (f) showed an enlarged view of interaction zone closed to plasma membrane (Bar=5 μm). Empty n/c YPF was used as negative controls (d and g).

(h) Calcium dependent OsCaM1-OsIQD14 interaction *in vitro*. GST beads loaded with GST-tagged Calmodulin (OsCaM1) were incubated with OsIQD14-His protein at 4ºC in the presence of 2 mM $CaCl_2$ or 5 mM EGTA. Pellet (GST-OsCaM1 beads) fraction was detected by probing with His antibody (top) or stained with Coomassie brilliant blue (bottom).

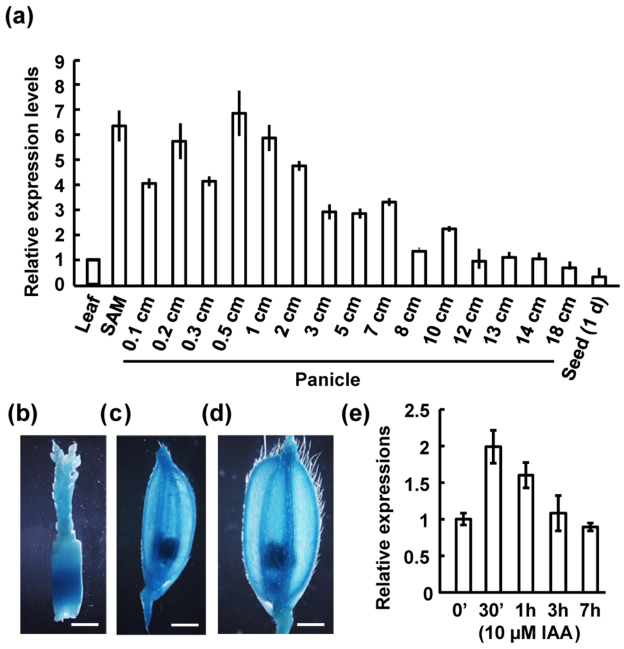

pbi_13279_f1.tif

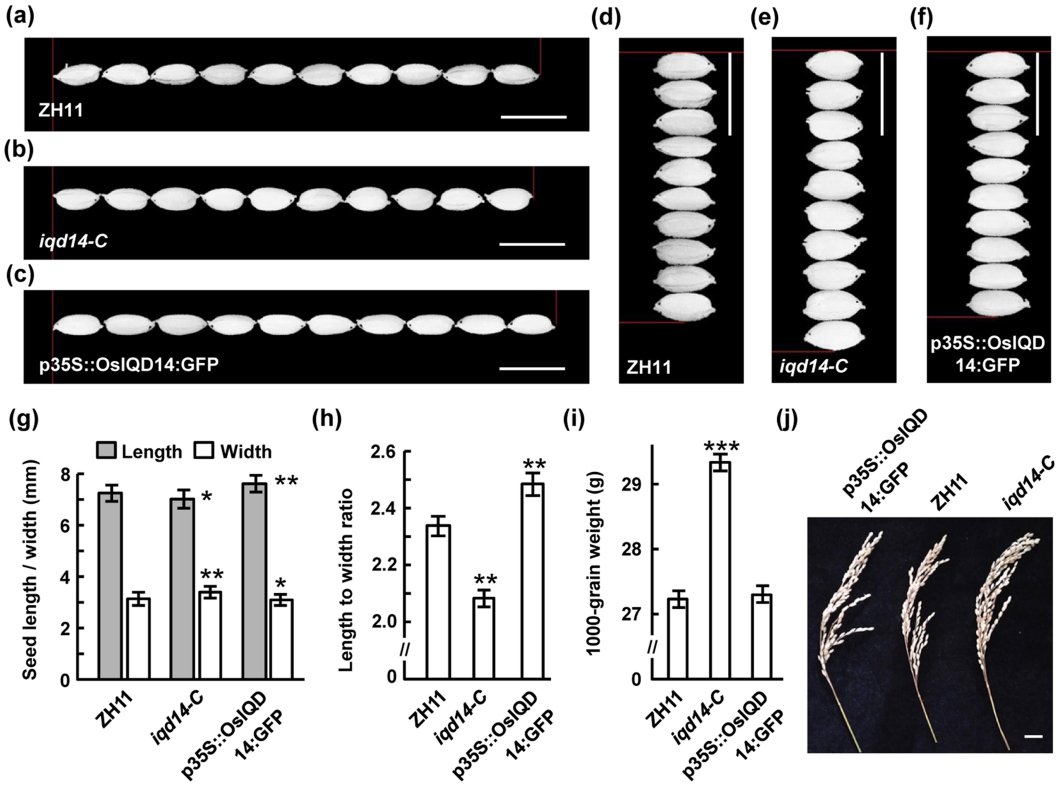

pbi_13279_f2.tif

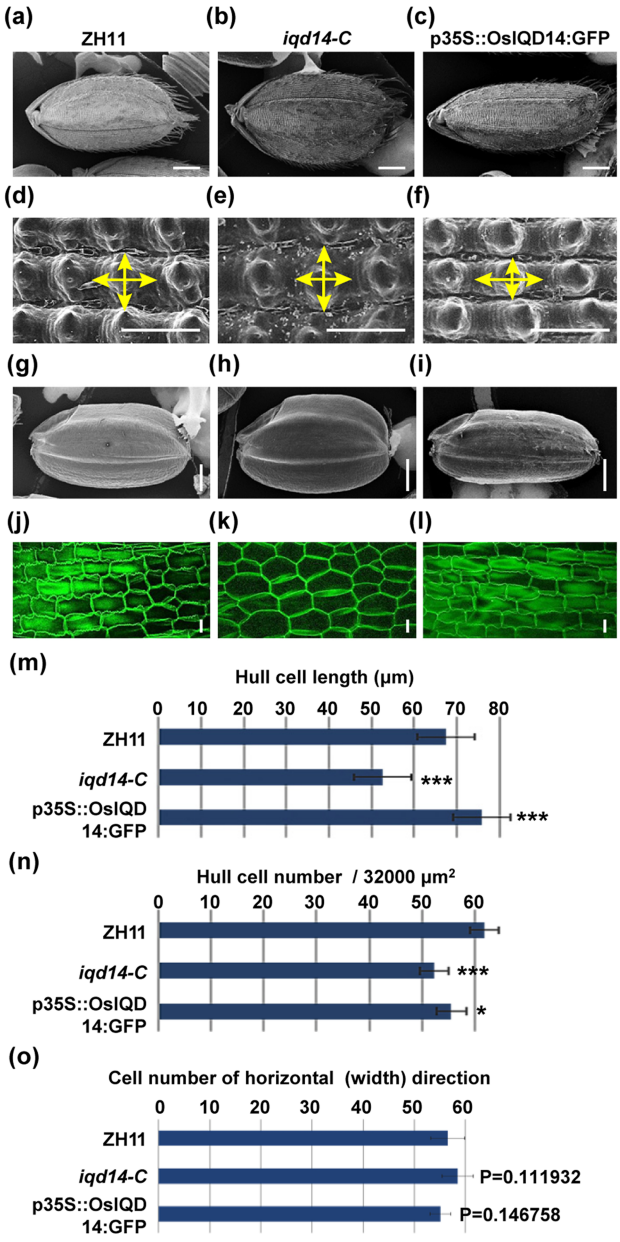

pbi_13279_f3.tif

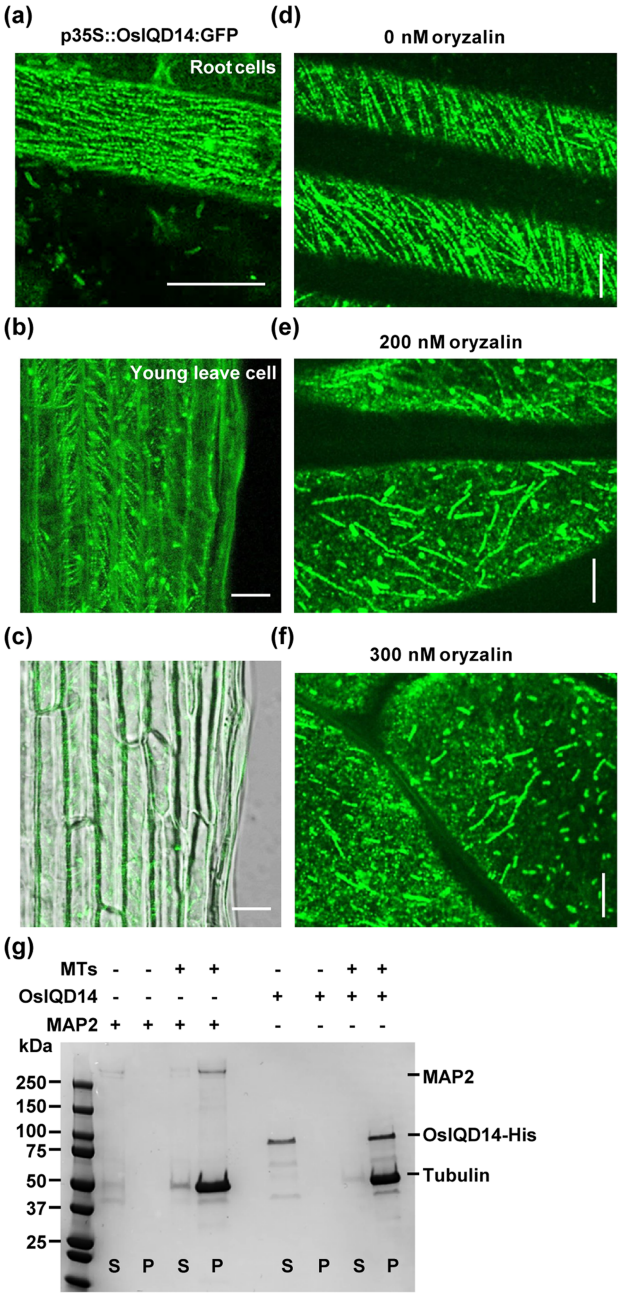

pbi_13279_f4.tif

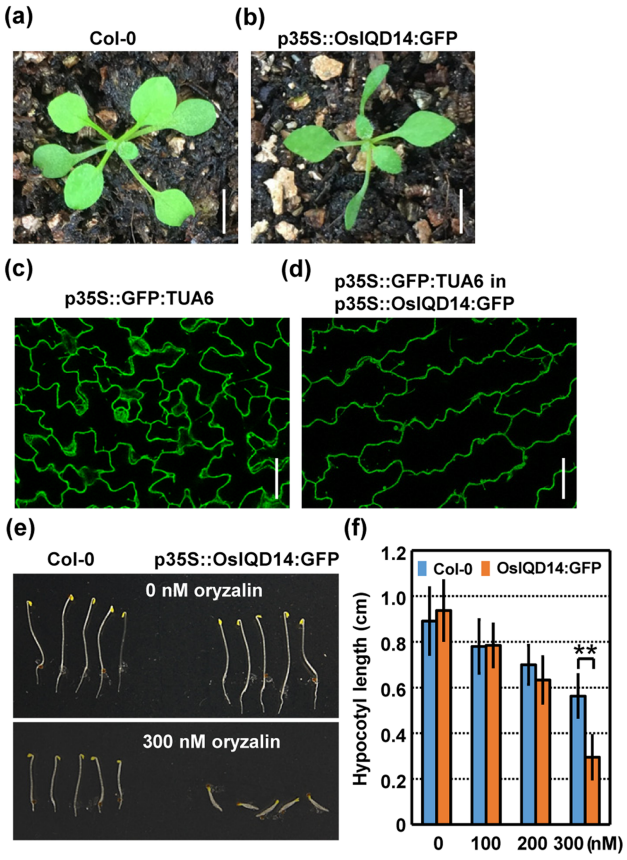

pbi_13279_f5.tif

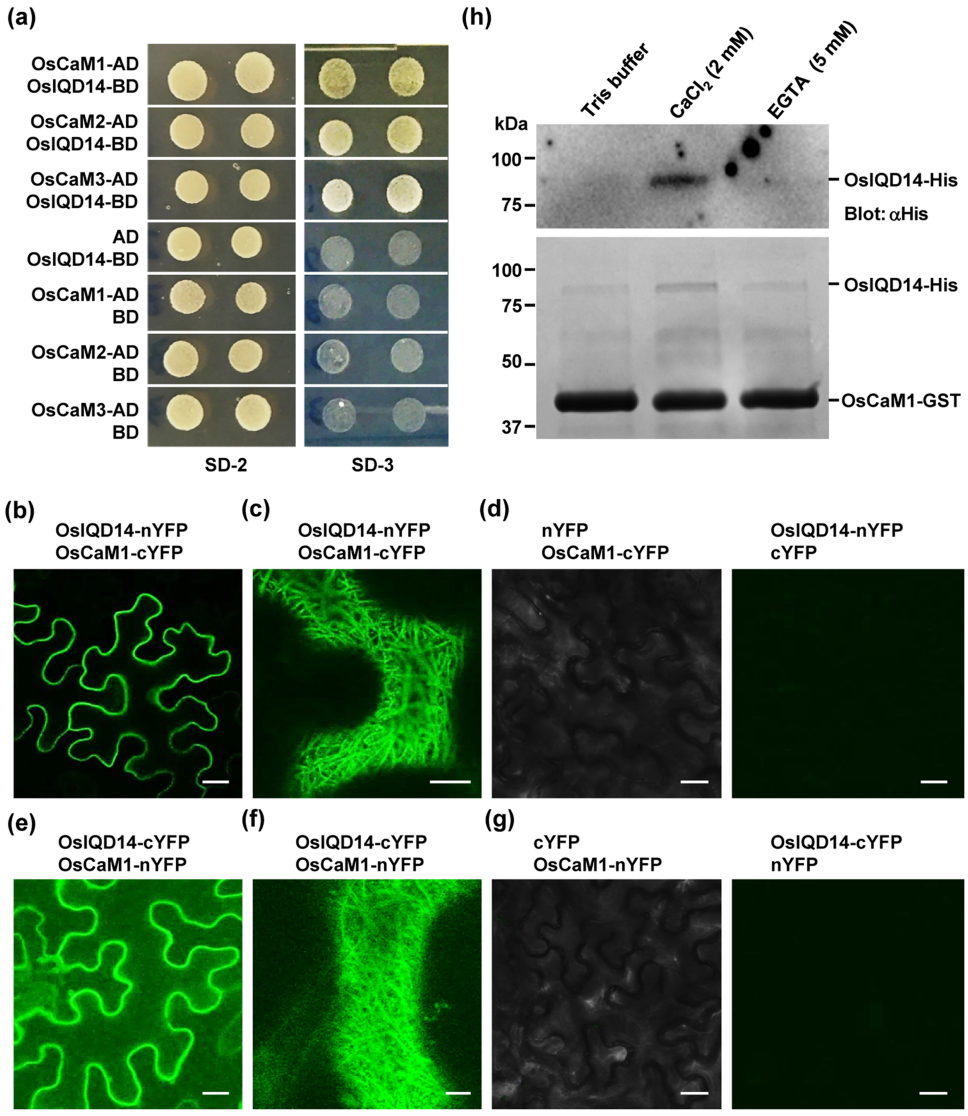

pbi_13279_f6.tif